



Dynamic response of asphalt pavement under vibration rolling load: Theory and calibration

Shi-Ping Wang^a, Han-Cheng Dan^{a,*}, Liang Li^{a,**}, Xiang Liu^b, Zhi Zhang^a

^a School of Civil Engineering, Central South University, Hunan, Changsha, 410075, China

^b School of Traffic & Transportation Engineering, Central South University, Hunan, Changsha, 410075, China

ARTICLE INFO

Keywords:

Vibration load
Dynamic response
Stiffness matrix
Dynamic stiffness method
Fourier transform method

ABSTRACT

Vibrating compaction is a critical procedure to guarantee the quality of asphalt pavement, and the dynamic response of asphalt pavement is a complicate problem in the process of vibration rolling. This paper aims to theoretically investigate the dynamic response regulation and influencing factors of pavement under the moving vibration load. Firstly, based on the viscoelastic theory of multi-layer system, the dynamic response governing equation of asphalt pavement is established under the vibration load, the governing equation was then simplified by the two-dimensional Fourier transform method. Further, the stiffness matrices of the single-layer and multi-layer pavement structures are obtained by using the dynamic stiffness method. Consequently, the exact solution is obtained for the plane strain problem by programming and validated with the finite element results, which is proved to be more efficient in the calculation. Moreover, the model is calibrated by the field test to determine the wave number and dynamic modulus during the vibration rolling process. Subsequently, the effects of material and load frequency are investigated on the dynamic response in terms of acceleration and displacement. The results show that both of the acceleration and displacement of pavement surface vibrate periodically with the vibrating load, and the changing regulations of the acceleration and displacement with loading time can be divided into three stages corresponding to the engineering practice such as rapid decline, slow decline and stable stages. Finally, the influencing factors are analyzed in terms of the modulus of materials (i.e., surface course and base course) and the frequency of load. It shows that the peak values of acceleration and displacement of the pavement surface change significantly and nonlinearly with the material modulus in the form of power function. Meanwhile, the influence of vibrating frequency is also significant and a quadratic relationship between the acceleration/displacement and frequency. This paper provides an insight into understanding the dynamic response of pavement under vibration rolling condition to some extent, and potentially provides theoretical and technical support for accurately determining and modifying some indexes that characterize the compaction degree of asphalt pavement.

1. Introduction

Asphalt pavement is widely used in the construction of highway engineering projects in the world. The transportation of the large traffic volume, heavy vehicles and high driving speed put forward higher requirements for the strength and durability of asphalt pavement structure [1–3]. Generally speaking, insufficient strength and poor durability are important reason to asphalt pavement diseases such as rutting, cracks, water damage etc. [4–7]. To a large extent, these diseases closely relate

to the construction quality of asphalt pavement, and the compaction quality will directly affect the quality of asphalt pavement [4,8–12]. Therefore, how to guarantee the compaction quality of pavement is a significant issue concerned by pavement engineers and researchers. Although the problem of pavement compaction has existed for a long time, more researches were carried out from the view of materials and technology [13,14], and not enough attention is paid to the mechanical problems in the compaction process of asphalt pavement. Therefore, it is an obstacle to fully understand the dynamic regulation of a pavement

* Corresponding author.

** Corresponding author.

E-mail addresses: csu-shipingwang@csu.edu.cn (S.-P. Wang), danhancheng@csu.edu.cn (H.-C. Dan), liliang_csu@126.com (L. Li), xiangliu@csu.edu.cn (X. Liu), zz768956@csu.edu.cn (Z. Zhang).

<https://doi.org/10.1016/j.soildyn.2021.106633>

Received 23 August 2020; Received in revised form 22 January 2021; Accepted 28 January 2021

Available online 13 February 2021

0267-7261/© 2021 Elsevier Ltd. All rights reserved.

compaction. On the one hand, it is not conducive to improving the degree of pavement compaction in terms of economy and efficiency; On the other hand, continuous compaction technology is also based on the weak theoretical foundation at present thereby hindering its development and application [12].

As we all know, vibratory roller has the characteristics of good compaction effect, large influence depth and high production efficiency, which greatly improves the compaction degree of asphalt mixture. Therefore, the vibratory roller is widely applied in the compaction engineering of asphalt pavement [11,15]. In the process of vibratory compaction of asphalt pavement, the vibratory roller not only runs on the surface of asphalt pavement at a certain speed, but also vibrates up and down at a certain frequency. Therefore, compared with the traffic load, the dynamic response of asphalt pavement in the process of vibratory rolling is definitely different and special. Many researchers carried out investigation on the dynamic response of asphalt pavement under various types of loads, and those methods are roughly divided into two categories such as analytical method and numerical simulation [16–23]. The experimental studies are very few to be referred [24–26]. For the category of analytical method, the differential governing equation is usually established and the analytical and semi-analytical solutions of pavement dynamic response were obtained by means of integral transformation. For example, Steenbergen [27], Kononov [28] regarded the pavement as a beam or slab on a half-space multi-layer system to establish the model of road structure, while Dong [29], Zhi Lyu [19], Lin [30], Grundmann [31] assumed that the pavement is the top layer on the half-space multi-layer system. For the simplification of the moving load, Xu [32,33], Lu [34], Jin [35], etc. Simplified the moving traffic load to a moving concentrated load or uniform load, and Zhi Lyu [19], Mesgouze [36] simplified to be an ordinary harmonic load. Then, through the integral transformation of the time and space vectors, the governing equation under the moving load is transformed and the analytical solution or semi-analytical solution can be obtained.

Among these analytical methods, the most regarded the traffic load as moving concentrated and uniform load or moving loads that change harmonically with time. The study on vibration of pavement mainly considered the pavement roughness [19], but few researches investigated the characteristics of dynamic response in the process of vibration compaction of pavement because the use of analytical method is closely related to the complexity of the model itself [16,19]. In order to consider more complex situations, many researchers applied the finite element method to simulate the response of pavement under various dynamic loads. Maoyun Li [21] established the finite element model of viscoelastic and nonlinear materials for the dynamic response of flexible pavement under load of FWD to carry out parameter analysis. For the case of moving load, Niki D. Beskou [37] established a viscoelastic material model of surface layer (asphalt concrete) by using ANSYS software and time domain finite element method. The elastic model and viscoelastic model are compared and analyzed under static or dynamic vehicle load on the flexible pavement. Pengfei Liu et al. [16] utilized the semi-analytical finite element method to compile the corresponding program, and employed the finite element software SAFEM to model and calculate the asphalt pavement under heavy traffic load. Ogoubi [22] adopted implicit dynamic analysis to establish a 3D viscoelastic finite element model. Syed [38] established a linear model to represent the dynamics of road rollers and asphalt pavement, and asphalt pavement was represented as a collection of mechanical units with viscoelastic-plastic properties. The presented model was validated by the data collected in the field compaction, which can better simulate the compaction process of asphalt mixture under field vibratory roller. From the above researches, although finite element software was applied to accurately simulate the dynamic response of pavement under dynamic load to some extent, the finite element simulation calculation is time-consuming and inefficient in general. At present, the literature on the dynamic response of asphalt pavement structure under the combined action of moving and vibration loads is relatively scarce, especially

taking the process of vibration compaction of asphalt pavement needs to be carried out in theoretical.

Hence, taking the characteristics of moving vibration load into account in the vibrating compaction, this paper aims to study the dynamic response regulation and the influencing effectors on the asphalt pavement in the compaction process. The viscoelasticity theory of multi-layer system can be adopted to establish the governing equation of multi-layer pavement under dynamic load, and the Fourier transform method and dynamic stiffness method will be employed to seek for the analytical solution so as to achieve the purpose of fast and efficient calculation. Moreover, the dynamic response of asphalt pavement can be then investigated under the action of vibratory roller in terms of the significance of influencing factors.

2. Methodology

2.1. Assumptions

After the asphalt mixture being paved, the asphalt mixture has a compactness of about 90% [15]. From a certain observation point of the pavement surface, the action time of the vibratory roller is about 0.1–0.2 s, and the vibration frequency of load is frequently controlled at about 40 Hz - 50Hz [39], the plastic deformation in the finite acting time of the vibratory roller is very small, and the dynamic response process is thus regarded as the viscoelastic vibration. Before model establishment, the following assumptions need to be introduced.

- (1) The vibration system of asphalt pavement structure and vibratory roller is linear;
- (2) The structural layers underneath surface course are homogeneous and isotropic elastic materials;
- (3) The constitutive properties of structural layer satisfy Hooke's law;
- (4) The displacement at a certain depth of the pavement structure is zero.

It should be pointed out that the moving speed of the vibratory roller is about 3.6 km/h~5.4 km/h [40], which can be negligible compared with the vibration speed or frequency of the vibratory roller. Therefore, it is assumed that the load vibrates freely on the road surface with a sine wave and the load position keep fixed. The pavement response with time can be illustrated according to different positions which is expressed by $x = v \cdot t$ (v is the moving speed of the road roller, t is the sampling time, and x is the distance to the observation point) [17].

2.2. Governing equations

The asphalt pavement system is regarded as a multi-layer linear elasticity, and the theoretical derivation is carried out based on the theory of viscoelastic layered system [41]. The schematic diagram of the two-dimensional multilayer system in the Cartesian coordinate system is shown in Fig. 1. The observation point on the top surface is the origin of coordinates, and the positive direction of the x and z axis are in line with the direction of load movement and pavement depth, respectively.

For asphalt pavement, under the action of vibration load, the displacement of pavement can be decomposed into the x and z components which horizontal displacement $u(x, z, t)$ and vertical displacement $w(x, z, t)$. Likewise, the normal stress of pavement in x -axis and z -axis directions are $\sigma_x(x, z, t)$ and $\sigma_z(x, z, t)$ respectively. Accordingly, the force balance equation is obtained as follows:

$$\begin{cases} \frac{\partial \sigma_x(x, z, t)}{\partial x} + \frac{\partial \tau_{zx}(x, z, t)}{\partial z} = \rho \frac{\partial^2 u(x, z, t)}{\partial t^2} \\ \frac{\partial \tau_{xz}(x, z, t)}{\partial x} + \frac{\partial \sigma_z(x, z, t)}{\partial z} = \rho \frac{\partial^2 w(x, z, t)}{\partial t^2} \end{cases} \quad (1)$$

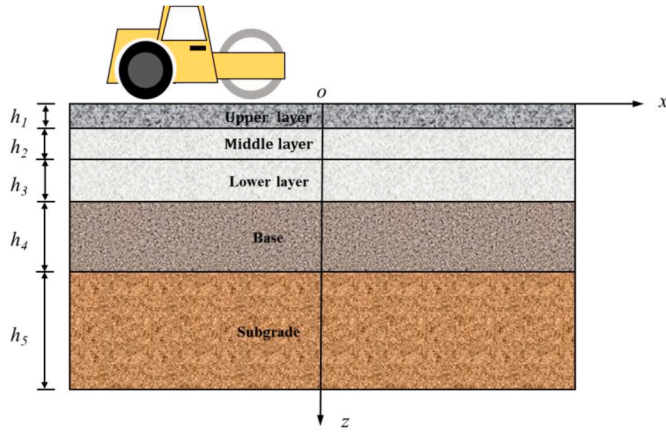


Fig. 1. Schematic diagram of 2D multi-layer system of pavement.

where ρ is the density of pavement material, and $\tau_{xz}(x, z, t) = \tau_{zx}(x, z, t)$ is the shear stress in xz plane of the pavement structure.

In the two-dimensional multi-layer elastic system of pavement, the physical and geometric equations of the plane strain problem are as follows:

$$\begin{cases} \varepsilon_x(x, z, t) = \frac{1-\nu^2}{E} \left(\sigma_x(x, z, t) - \frac{\nu}{1-\nu} \sigma_z(x, z, t) \right) \\ \varepsilon_z(x, z, t) = \frac{1-\nu^2}{E} \left(\sigma_z(x, z, t) - \frac{\nu}{1-\nu} \sigma_x(x, z, t) \right) \\ \gamma_{xz}(x, z, t) = \frac{1}{G} \tau_{xz}(x, z, t) \end{cases} \quad (2)$$

$$\begin{cases} \varepsilon_x(x, z, t) = \frac{\partial u(x, z, t)}{\partial x} \\ \varepsilon_z(x, z, t) = \frac{\partial w(x, z, t)}{\partial z} \\ \gamma_{xz}(x, z, t) = \frac{\partial u(x, z, t)}{\partial z} + \frac{\partial w(x, z, t)}{\partial x} \end{cases} \quad (3)$$

where ν , E and G are the Poisson ratio, Young's elastic modulus and shear modulus of the material, respectively.

According to Fourier transform method, equations (1)–(3) in time domain can be transformed into that in the frequency domain, which can be given as follows:

$$\begin{cases} \frac{\partial \tilde{\sigma}_x(x, z, \xi)}{\partial x} + \frac{\partial \tilde{\tau}_{zx}(x, z, \xi)}{\partial z} + \rho \xi^2 \tilde{u}(x, z, \xi) = 0 \\ \frac{\partial \tilde{\tau}_{xz}(x, z, \xi)}{\partial x} + \frac{\partial \tilde{\sigma}_z(x, z, \xi)}{\partial z} + \rho \xi^2 \tilde{w}(x, z, \xi) = 0 \end{cases} \quad (4)$$

$$\begin{cases} \tilde{\varepsilon}_x(x, z, \xi) = \frac{1-\nu^2}{E} \left(\tilde{\sigma}_x(x, z, \xi) - \frac{\nu}{1-\nu} \tilde{\sigma}_z(x, z, \xi) \right) \\ \tilde{\varepsilon}_z(x, z, \xi) = \frac{1-\nu^2}{E} \left(\tilde{\sigma}_z(x, z, \xi) - \frac{\nu}{1-\nu} \tilde{\sigma}_x(x, z, \xi) \right) \\ \tilde{\gamma}_{xz}(x, z, \xi) = \frac{1}{G} \tilde{\tau}_{xz}(x, z, \xi) \end{cases} \quad (5)$$

$$\begin{cases} \tilde{\varepsilon}_x(x, z, \xi) = \frac{\partial \tilde{u}(x, z, \xi)}{\partial x} \\ \tilde{\varepsilon}_z(x, z, \xi) = \frac{\partial \tilde{w}(x, z, \xi)}{\partial z} \\ \tilde{\gamma}_{xz}(x, z, \xi) = \frac{\partial \tilde{u}(x, z, \xi)}{\partial z} + \frac{\partial \tilde{w}(x, z, \xi)}{\partial x} \end{cases} \quad (6)$$

It can be define that

$$\begin{cases} \lambda = \frac{\nu E(1+\eta j)}{(1+\nu)(1-2\nu)} \\ G = \frac{E(1+\eta j)}{2(1+\nu)} \end{cases} \quad (7)$$

in which η is the material damping coefficient and it is not considered in this paper because its value cannot be determined under high temperature during the pavement compaction process.

The following equations can be obtained by combining equations (4)–(7) as follows.

$$\tilde{\sigma}_z(x, z, \xi) = (\lambda + 2G) \frac{\partial \tilde{w}(x, z, \xi)}{\partial z} + \lambda \frac{\partial \tilde{u}(x, z, \xi)}{\partial x} \quad (8)$$

$$\tilde{\tau}_{zx}(x, z, \xi) = G \left(\frac{\partial \tilde{w}(x, z, \xi)}{\partial x} + \frac{\partial \tilde{u}(x, z, \xi)}{\partial z} \right) \quad (9)$$

$$\tilde{\sigma}_x(x, z, \xi) = (\lambda + 2G) \frac{\partial \tilde{u}(x, z, \xi)}{\partial x} + \lambda \frac{\partial \tilde{w}(x, z, \xi)}{\partial z} \quad (10)$$

Taking the derivative of equation (8) with respect to x , we have

$$\frac{\partial^2 \tilde{w}(x, z, \xi)}{\partial z \partial x} = \frac{1}{(\lambda + 2G)} \frac{\partial \tilde{\sigma}_z(x, z, \xi)}{\partial x} - \frac{\lambda}{(\lambda + 2G)} \frac{\partial^2 \tilde{u}(x, z, \xi)}{\partial x^2} \quad (11)$$

Then taking the derivative of equation (10) with respect to x , and then combing with equation (11), it can be obtained

$$\frac{\partial \tilde{\sigma}_x(x, z, \xi)}{\partial x} = \frac{4G(\lambda + G)}{\lambda + 2G} \frac{\partial^2 \tilde{u}(x, z, \xi)}{\partial x^2} + \frac{\lambda}{\lambda + 2G} \frac{\partial \tilde{\sigma}_z(x, z, \xi)}{\partial x} \quad (12)$$

Performing the Fourier transform on the spatial domain of stress and displacement in x and z directions, the equation set (4) can be simplified as

$$\begin{cases} \frac{\partial \tilde{\sigma}_z(k, z, \xi)}{\partial z} = -k j \tilde{\tau}_{zx}(k, z, \xi) - \rho \xi^2 \tilde{w}(k, z, \xi) \\ \frac{\partial j \tilde{\tau}_{xz}(k, z, \xi)}{\partial z} = \frac{\lambda k}{\lambda + 2G} \tilde{\sigma}_z(k, z, \xi) + \left[\frac{4G(\lambda + G)k^2}{\lambda + 2G} - \rho \xi^2 \right] j \tilde{u}(k, z, \xi) \end{cases} \quad (13)$$

Therefore, equation (8) and equation (9) can be simplified as

$$\frac{\partial \tilde{w}(k, z, \xi)}{\partial z} = \frac{1}{\lambda + 2G} \tilde{\sigma}_z(k, z, \xi) - \frac{\lambda k}{\lambda + 2G} j \tilde{u}(k, z, \xi) \quad (14)$$

$$\frac{\partial j \tilde{u}(k, z, \xi)}{\partial z} = \frac{j \tilde{\tau}_{xz}(k, z, \xi)}{G} + k \tilde{w}(k, z, \xi) \quad (15)$$

By combining equations (13)–(15), the governing equation after performing the Fourier transform can be given as follows.

$$\begin{cases} \frac{\partial \tilde{\sigma}_z(k, z, \xi)}{\partial z} = -k j \tilde{\tau}_{zx}(k, z, \xi) - \rho \xi^2 \tilde{w}(k, z, \xi) \\ \frac{\partial j \tilde{\tau}_{xz}(k, z, \xi)}{\partial z} = \frac{\lambda k}{\lambda + 2G} \tilde{\sigma}_z(k, z, \xi) + \left[\frac{4G(\lambda + G)k^2}{\lambda + 2G} - \rho \xi^2 \right] j \tilde{u}(k, z, \xi) \\ \frac{\partial \tilde{w}(k, z, \xi)}{\partial z} = \frac{1}{\lambda + 2G} \tilde{\sigma}_z(k, z, \xi) - \frac{\lambda k}{\lambda + 2G} j \tilde{u}(k, z, \xi) \\ \frac{\partial j \tilde{u}(k, z, \xi)}{\partial z} = \frac{j \tilde{\tau}_{xz}(k, z, \xi)}{G} + k \tilde{w}(k, z, \xi) \end{cases} \quad (16)$$

When the equation set (16) is sorted out into matrix form, the following equation (17) set can be obtained.

$$\frac{\partial}{\partial z} \begin{bmatrix} \tilde{\sigma}_z(k, z, \xi) \\ \tilde{f}\tilde{r}_{xz}(k, z, \xi) \\ \tilde{w}(k, z, \xi) \\ \tilde{j}\tilde{u}(k, z, \xi) \end{bmatrix} = \begin{bmatrix} 0 & -k & -\rho\xi^2 & 0 \\ \frac{\lambda k}{\lambda + 2G} & 0 & 0 & \frac{4G(\lambda + G)k^2}{\lambda + 2G} - \rho\xi^2 \\ \frac{1}{\lambda + 2G} & 0 & 0 & \frac{\lambda k}{\lambda + 2G} \\ 0 & 1/G & k & 0 \end{bmatrix} \begin{bmatrix} \tilde{\sigma}_z(k, z, \xi) \\ \tilde{f}\tilde{r}_{xz}(k, z, \xi) \\ \tilde{w}(k, z, \xi) \\ \tilde{j}\tilde{u}(k, z, \xi) \end{bmatrix} \quad (17)$$

2.3. Stiffness matrix for one layer

Based on the established governing equation (17), it is simplified in the form of matrix to facilitate the derivation of the model solution. Firstly, we define

$$B = \begin{bmatrix} 0 & -k & -\rho\xi^2 & 0 \\ \frac{\lambda k}{\lambda + 2G} & 0 & 0 & \frac{4G(\lambda + G)k^2}{\lambda + 2G} - \rho\xi^2 \\ \frac{1}{\lambda + 2G} & 0 & 0 & \frac{\lambda k}{\lambda + 2G} \\ 0 & 1/G & k & 0 \end{bmatrix}, \quad (18)$$

and equation (17) can be rewritten as

$$\frac{\partial}{\partial z} \begin{bmatrix} \tilde{\sigma}_z(k, z, \xi) \\ \tilde{f}\tilde{r}_{xz}(k, z, \xi) \\ \tilde{w}(k, z, \xi) \\ \tilde{j}\tilde{u}(k, z, \xi) \end{bmatrix} = B \times \begin{bmatrix} \tilde{\sigma}_z(k, z, \xi) \\ \tilde{f}\tilde{r}_{xz}(k, z, \xi) \\ \tilde{w}(k, z, \xi) \\ \tilde{j}\tilde{u}(k, z, \xi) \end{bmatrix} \quad (19)$$

It can be seen from Fig. 1 that the boundary condition at the top surface can be expressed by $[\tilde{\sigma}_z(k, 0, \xi), \tilde{f}\tilde{r}_{xz}(k, 0, \xi), \tilde{w}(k, 0, \xi), \tilde{j}\tilde{u}(k, 0, \xi)]^T$, and the boundary condition at $h = h_1$ is $[\tilde{\sigma}_z(k, h_1, \xi), \tilde{f}\tilde{r}_{xz}(k, h_1, \xi), \tilde{w}(k, h_1, \xi), \tilde{j}\tilde{u}(k, h_1, \xi)]^T$. Therefore, equation (19) can be solved directly according to the above boundary conditions.

$$\begin{bmatrix} \tilde{\sigma}_z(k, h_1, \xi) \\ \tilde{f}\tilde{r}_{xz}(k, h_1, \xi) \\ \tilde{w}(k, h_1, \xi) \\ \tilde{j}\tilde{u}(k, h_1, \xi) \end{bmatrix} = e^{Bh_1} \times \begin{bmatrix} \tilde{\sigma}_z(k, 0, \xi) \\ \tilde{f}\tilde{r}_{xz}(k, 0, \xi) \\ \tilde{w}(k, 0, \xi) \\ \tilde{j}\tilde{u}(k, 0, \xi) \end{bmatrix} \quad (20)$$

Define $T = e^{Bh_1}$ and combine with the block matrix algorithm, equation (21) can be obtained.

$$\begin{bmatrix} \tilde{\sigma}_z(k, h_1, \xi) \\ \tilde{f}\tilde{r}_{xz}(k, h_1, \xi) \\ \tilde{w}(k, h_1, \xi) \\ \tilde{j}\tilde{u}(k, h_1, \xi) \end{bmatrix} = \begin{bmatrix} [T_{11}] & [T_{12}] \\ [T_{21}] & [T_{22}] \end{bmatrix} \begin{bmatrix} \tilde{\sigma}_z(k, 0, \xi) \\ \tilde{f}\tilde{r}_{xz}(k, 0, \xi) \\ \tilde{w}(k, 0, \xi) \\ \tilde{j}\tilde{u}(k, 0, \xi) \end{bmatrix} \quad (21)$$

According to the relationship between the stress and displacement, the following equation holds.

$$\begin{bmatrix} -\tilde{\sigma}_z(k, 0, \xi) \\ -\tilde{f}\tilde{r}_{xz}(k, 0, \xi) \\ \tilde{\sigma}_z(k, h_1, \xi) \\ \tilde{f}\tilde{r}_{xz}(k, h_1, \xi) \end{bmatrix} = \begin{bmatrix} T_{21}^{-1}T_{22} & -T_{21}^{-1} \\ T_{12} - T_{11}T_{21}^{-1}T_{22} & T_{11}T_{21}^{-1} \end{bmatrix} \times \begin{bmatrix} \tilde{w}(k, 0, \xi) \\ \tilde{j}\tilde{u}(k, 0, \xi) \\ \tilde{w}(k, h_1, \xi) \\ \tilde{j}\tilde{u}(k, h_1, \xi) \end{bmatrix} \quad (22)$$

Here, the first term on the right side of equation (22) is the stiffness matrix, and it is defined by

$$[S] = \begin{bmatrix} [T_{21}^{-1}T_{22}] & [-T_{21}^{-1}] \\ [T_{12} - T_{11}T_{21}^{-1}T_{22}] & [T_{11}T_{21}^{-1}] \end{bmatrix} = \begin{bmatrix} [S_{11}] & [S_{12}] \\ [S_{21}] & [S_{22}] \end{bmatrix} \quad (23)$$

2.4. Stiffness matrix for multiple layers

According to the schematic diagram of the pavement structure (Fig. 1), several layers with different materials are integrated to construct the pavement structure. Therefore, any two layers of the structure are selected for instance in order to obtain the global stiffness matrix of the asphalt pavement multi-layer system. For any two layers of pavement as shown in Fig. 2, the boundary condition at the top surface of the i -th layer is $z = H_{i-1}$, and the thickness $h = h_i$. Likewise, at the bottom surface of the layer $i + 1$, the displacement $z = H_{i+1}$, and the thickness $h = h_{i+1}$.

Therefore, the stiffness matrix for each layer is respectively given by equations (24) and (25) based on equation (22).

$$\begin{bmatrix} -\tilde{\sigma}_z(k, H_{i-1}, \xi) \\ -\tilde{f}\tilde{r}_{xz}(k, H_{i-1}, \xi) \\ \tilde{\sigma}_z(k, H_i, \xi) \\ \tilde{f}\tilde{r}_{xz}(k, H_i, \xi) \end{bmatrix} = \begin{bmatrix} [S_{11}^i] & [S_{12}^i] \\ [S_{21}^i] & [S_{22}^i] \end{bmatrix} \times \begin{bmatrix} \tilde{w}(k, H_{i-1}, \xi) \\ \tilde{j}\tilde{u}(k, H_{i-1}, \xi) \\ \tilde{w}(k, H_i, \xi) \\ \tilde{j}\tilde{u}(k, H_i, \xi) \end{bmatrix} \quad (24)$$

$$\begin{bmatrix} -\tilde{\sigma}_z(k, H_i, \xi) \\ -\tilde{f}\tilde{r}_{xz}(k, H_i, \xi) \\ \tilde{\sigma}_z(k, H_{i+1}, \xi) \\ \tilde{f}\tilde{r}_{xz}(k, H_{i+1}, \xi) \end{bmatrix} = \begin{bmatrix} [S_{11}^{i+1}] & [S_{12}^{i+1}] \\ [S_{21}^{i+1}] & [S_{22}^{i+1}] \end{bmatrix} \times \begin{bmatrix} \tilde{w}(k, H_i, \xi) \\ \tilde{j}\tilde{u}(k, H_i, \xi) \\ \tilde{w}(k, H_{i+1}, \xi) \\ \tilde{j}\tilde{u}(k, H_{i+1}, \xi) \end{bmatrix} \quad (25)$$

in which the superscripts (e.g., $i, i+1$) indicate the layer No.

According to the assumption that the layers of the structure are in complete contact with each other, and the stress and displacement are continuous [42], we thus have

$$\begin{bmatrix} 0 \\ 0 \end{bmatrix} = [S_{21}^i] \times \begin{bmatrix} \tilde{w}(k, H_{i-1}, \xi) \\ \tilde{j}\tilde{u}(k, H_{i-1}, \xi) \end{bmatrix} + ([S_{22}^i] + [S_{11}^{i+1}]) \times \begin{bmatrix} \tilde{w}(k, H_i, \xi) \\ \tilde{j}\tilde{u}(k, H_i, \xi) \end{bmatrix} + [S_{12}^{i+1}] \times \begin{bmatrix} \tilde{w}(k, H_{i+1}, \xi) \\ \tilde{j}\tilde{u}(k, H_{i+1}, \xi) \end{bmatrix} \quad (26)$$

Composing equations (24) to (26), we have

$$\begin{bmatrix} -\tilde{\sigma}_z(k, H_{i-1}, \xi) \\ -\tilde{f}\tilde{r}_{xz}(k, H_{i-1}, \xi) \\ 0 \\ 0 \\ \tilde{\sigma}_z(k, H_{i+1}, \xi) \\ \tilde{f}\tilde{r}_{xz}(k, H_{i+1}, \xi) \end{bmatrix} = \begin{bmatrix} [S_{11}^i] & [S_{12}^i] & 0 \\ [S_{21}^i] & [S_{22}^i] + [S_{11}^{i+1}] & [S_{12}^{i+1}] \\ 0 & [S_{21}^{i+1}] & [S_{22}^{i+1}] \end{bmatrix} \times \begin{bmatrix} \tilde{w}(k, H_{i-1}, \xi) \\ \tilde{j}\tilde{u}(k, H_{i-1}, \xi) \\ \tilde{w}(k, H_i, \xi) \\ \tilde{j}\tilde{u}(k, H_i, \xi) \\ \tilde{w}(k, H_{i+1}, \xi) \\ \tilde{j}\tilde{u}(k, H_{i+1}, \xi) \end{bmatrix} \quad (27)$$

Therefore, the global stiffness matrix of any two-layer structure is given by

$$[S] = \begin{bmatrix} [S_{11}^i] & [S_{12}^i] & 0 \\ [S_{21}^i] & [S_{22}^i] + [S_{11}^{i+1}] & [S_{12}^{i+1}] \\ 0 & [S_{21}^{i+1}] & [S_{22}^{i+1}] \end{bmatrix} \quad (28)$$

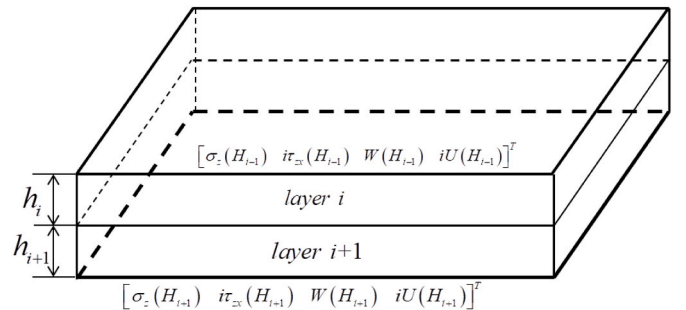


Fig. 2. Schematic diagram of any two-layer structure.

For the multi-layer system of asphalt pavement, the bottom layer is in complete contact with the rigid foundation bed, it can be inferred that there is a boundary condition at which the stress and displacement of the bottom is zero. Then the displacement and stress in the Fourier domain are also zero, from which the global stiffness matrix of the multi-layer system of asphalt pavement can be obtained accordingly.

$$\begin{bmatrix} f_1 \\ 0 \\ 0 \\ \vdots \\ 0 \\ f_{n+1} \end{bmatrix} = \begin{bmatrix} [S_{11}^1] & [S_{12}^1] & 0 & \cdots & 0 & 0 \\ [S_{21}^1] & [S_{22}^1 + S_{11}^2] & [S_{12}^2] & \cdots & 0 & 0 \\ 0 & [S_{21}^2] & [S_{22}^2 + S_{11}^3] & \cdots & 0 & 0 \\ \vdots & \vdots & \vdots & \ddots & \vdots & \vdots \\ 0 & 0 & 0 & \cdots & [S_{22}^{n-1} + S_{11}^n] & [S_{12}^n] \\ 0 & 0 & 0 & \cdots & [S_{21}^n] & [S_{22}^n] \end{bmatrix} \begin{bmatrix} d_1 \\ d_2 \\ d_3 \\ \vdots \\ d_n \\ d_{n+1} \end{bmatrix} \quad (29)$$

where, $f_1 = [-\tilde{\sigma}_z(k, 0, \xi), -\tilde{\tau}_{xz}(k, 0, \xi)]^T$, $d_i = [\tilde{w}(k, H_{i-1}, \xi), \tilde{u}(k, H_{i-1}, \xi)]^T$ and the subscripts i and n represent the i -th layer and layer number, respectively.

2.5. Vibration load

Obviously, the influence of load on the coupling between vibrating drum and pavement is very important. Generally speaking, the load distribution at the bottom of the vibrating drum is not uniform. That's to say the middle part of drum is larger and the edge part is smaller [11]. In addition, the contact between drum bottom and pavement surface is constantly changing during the vibration rolling process, which leads to the periodic change of contact stress. Therefore, in the two-dimensional case, considering the uneven distribution of load at the bottom of the vibrating drum, the distribution of contact force is regarded as a semi-ellipse model in this paper [43]. Furthermore, considering the vibration of the roller, it is assumed that the eccentric block in the vibratory roller rotates around the rotating shaft at a certain angular speed, making the eccentric block generate periodic rotation and vibration, as shown in Fig. 3.

Accordingly, the load function of vibratory roller is simplified to as follows [43].

$$P(x, t) = G_r + p(x, t) = G_r + \frac{b}{a} \sqrt{a^2 - (x - v_0 t)^2} \sin(\omega_0 t) \quad (30)$$

where, G_r is the gravity of roller, a is the half width of load, b is the load amplitude, v_0 is the speed of vibratory roller, and ω_0 is the angular frequency of rotor in the vibrating drum.

For the vibration rolling in the practical engineering, the moving speed of roller is about 4.5 km/h, which is far less than the transmission velocity of the vibration wave produced by the vibrating load in the asphalt mixture. Therefore, it can be considered that the speed of the vibratory roller is zero in the calculation, that is, the load function model of the exciting force is simplified by Ref. [44].

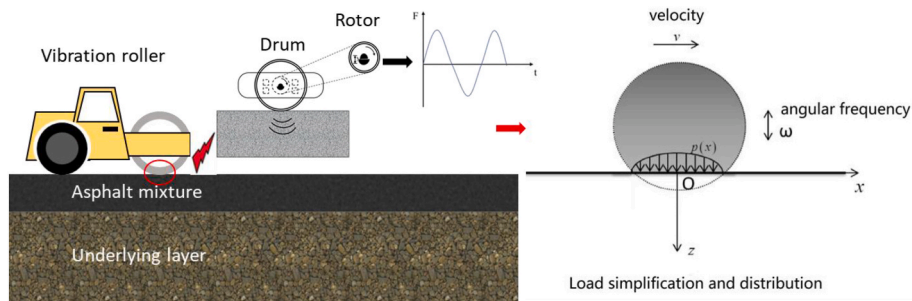


Fig. 3. Schematic diagram of load simplification and distribution.

$$p_c(x, t) = \frac{b}{a} \sqrt{a^2 - x^2} \sin(\omega_0 t) \quad (31)$$

Therefore, the expression of the vibration load can be simplified as

$$P_c(x, t) = G_r + p_c(x, t) = G_r + \frac{b}{a} \sqrt{a^2 - x^2} \sin(\omega_0 t) \quad (32)$$

2.6. Model solution

Herein, the two-dimensional Fourier transform in time domain and space domain is carried out to obtain the transformed expression of equation (32) in the frequency domain and wavenumber domain by the following equation.

$$\tilde{P}_c(k, \xi) = \int_{-\infty}^{+\infty} \int_{-\infty}^{+\infty} P_c(x, t) \exp[j(kx + \xi t)] dx dt \quad (33)$$

where, $\xi = \pi m/T$ and $k = \pi n/L$. The parameters T and L are the period and wave length of the load, respectively; if M and N are sampling points and spatial discrete points, respectively, then $m = 0, 1, 2, \dots, M$ and $n = 0, 1, 2, \dots, N$

Further, combining with the boundary conditions of multi-layer system of asphalt pavement, the numerical solution of the displacement equation (29), and then the solutions of displacement in time domain and space domain can be obtained by the two-dimensional inverse Fourier transform (IFT). The calculation program is compiled through MATLAB software integrating the *fft2* and *ifft2* functions, and the displacement $d = [d_1, d_2, \dots, d_n, d_{n+1}]^T$ for each layer can be obtained accordingly.

3. Model validation

3.1. Numerical comparison

(1) Comparison with the finite element method

As an auxiliary calculation method, the finite element method is often used for validation (e.g. Refs. [29,42,45–48]). To validate the model solution in this paper, the finite element method (FEM) is employed to calculate the vertical displacement of the top surface of asphalt pavement under the same conditions. A two-dimensional geometric model of 1040104 nodes is established by using the finite element software ABAQUS. The DLOAD subroutine is applied to simulate loading procedure of the vibratory roller. The mesh and geometric information are shown in Fig. 4, and the material and structure information are listed in Table 1.

The comparison of calculated displacement by the FEM and analytical method is shown in Fig. 5. It can be seen that the displacement curve of the pavement surface calculated by the presented method in this paper is basically consistent with that of the finite element method. For instance, the peak vertical displacement of the pavement surface

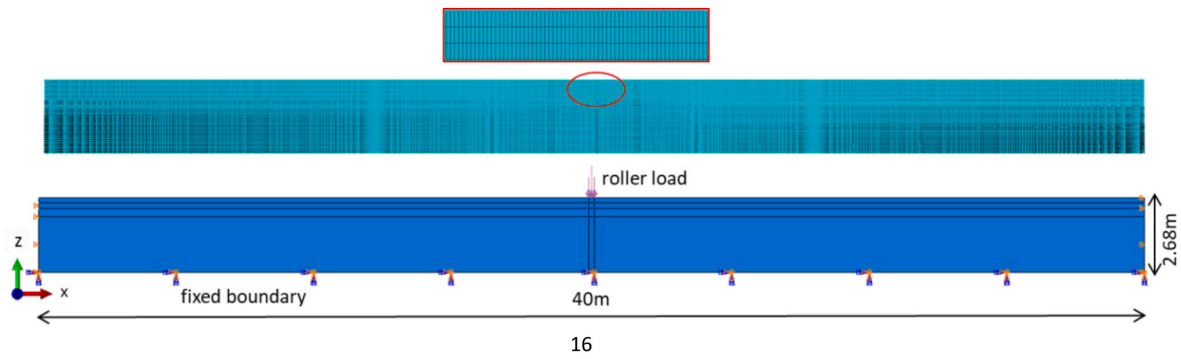


Fig. 4. The finite element model of asphalt pavement under vibrating load.

Table 1
Structure and material information for FEM simulation.

Materials	Thickness (cm)	Modulus (MPa)	Poisson's ratio	Density (kg/m ³)
Asphalt mixture	18	1400	0.3	2400
Cement stabilized macadam	20	1500	0.2	2300
Lime soil	30	550	0.35	2000
Subgrade soil	200	48	0.4	1900

$\nu_1 = \nu_2 = 0.25, \nu_3 = 0.35; \rho_1 = 3200 \text{ kg/m}^3, \rho_2 = 2100 \text{ kg/m}^3, \rho_3 = 1500 \text{ kg/m}^3$). The comparison is shown in Fig. 6 in terms of the vertical displacement in different time and it shows good agreement.

3.2. Field test calibration

(1) Experiment program

The pavement vibration rolling field test is performed on a lower course of an asphalt concrete pavement, with a thickness of 8 cm, in the Chongshui Expressway in Guangxi Province, China [50]. The compacted material is AC-25, whose gradation is presented in Fig. 7. The technical information of bituminous binder is listed in Table 2. The vibratory roller is BW203 AD-4 with double drums, and its actual working parameters are listed in Table 3.

The SmartRock sensor is embedded in the lower course of the pavement, approximately 20–30 mm to the top surface. For the data collection and sorting, the SmartRock sensor is so placed that its vertical direction (z), rolling direction (y), and lateral direction (x) coincided with the z-, y-, and x-axis, respectively, of the coordinate system of the sensor. The SmartRock data are collected by a wireless signal data receiver (Fig. 8). During the compaction process, the acceleration signal of the vibrating drum is collected by an acceleration sensor named HCF, which is fixed on the vibration shaft of the rolling drum, and received by the supporting USB gateway. The data accuracy of the HCF can also reach 0.01g. In the rolling direction, the data record area is selected approximately 25 m before and after the measuring point. After each rolling, a non-nuclear density meter is employed to detect the compactness of the compacted mixture near the measuring point. It need

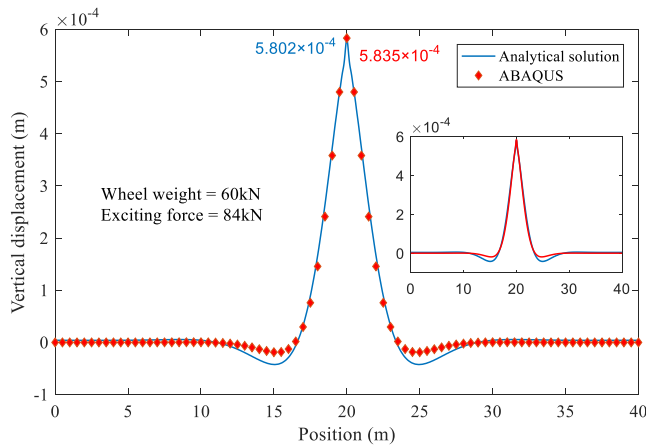


Fig. 5. The comparison between the FEM and analytical solution.

(2) Comparison with existing work

calculated by the analytical method and the FEM is 0.5835 mm and 0.5802 mm, respectively, with a difference of 0.57%. In addition, the influence range of load is basically the same, which is between 15.0 m and 25.0 m. Therefore, the comparison shows that the calculation method in this paper has better reliability with high accuracy. Moreover, it should be pointed out that although the finite element model adopts a density decreasing mesh, the calculation still takes more than 1 h; on the contrary, the calculation time of the analytical method in frequency domain is 22.6675 s and the inverse Fourier transform takes 0.618 s, thus the computational efficiency has been greatly improved.

The 2D dynamic response of a multilayer pavement half space system under a uniform load standing at origin has previously been determined analytically by Zhong et al. [49]. For the sake of comparison, the vibration rolling load in this paper is replaced by a uniform load according to the reference, and the parameters of the subgrade and pavement for calculation are selected according to Zhong et al. [49]. The parameters are listed herein (e.g., $p = 1 \text{ MPa}$, $\omega = \pi/10$, $P = p \cdot \sin(\omega t)$; $E_1 = 1000 \text{ MPa}$, $h_1 = 0.15 \text{ m}$; $E_2 = 300 \text{ MPa}$, $h_2 = 0.2 \text{ m}$; $R = 0.15 \text{ m}$, $E_3 = 95 \text{ MPa}$;

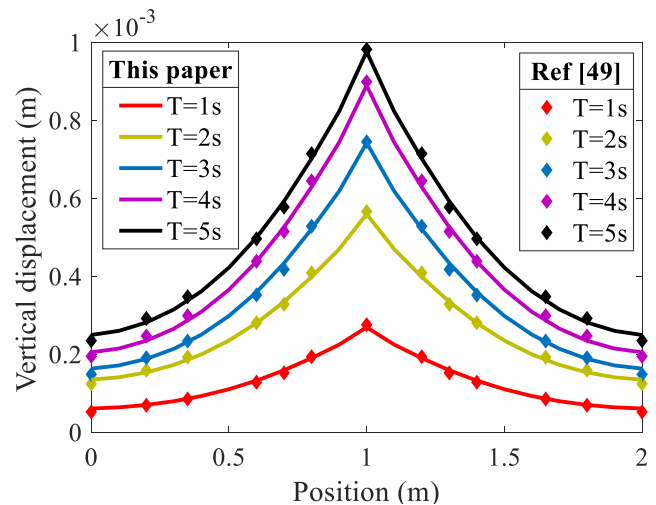


Fig. 6. Comparison between this paper and Ref [49].

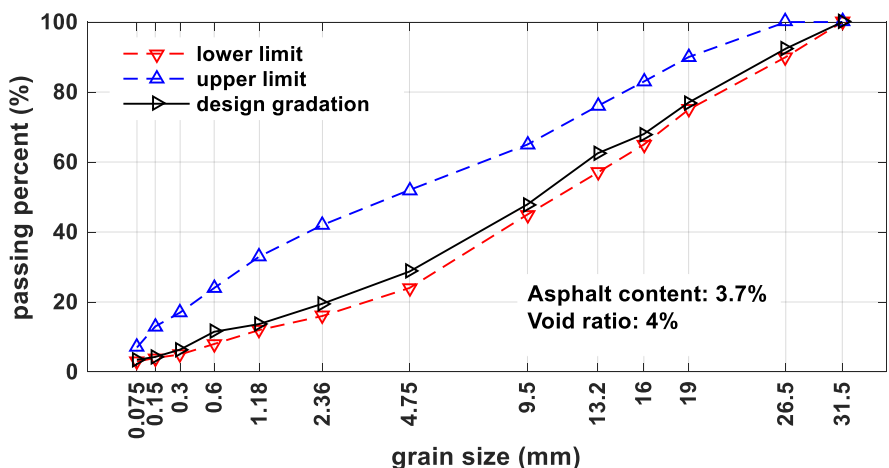


Fig. 7. Parameters of the material and grades.

Table 2
Technical information of bituminous binder.

Parameter	Value	Requirement	Methods (JTG E20-2019) [51]
Penetration (25°C, 100g, 5s)	63 (0.1 mm)	60-70 (0.1 mm)	T0604
Ductility (5 cm/min, 15°C)	≥100 (cm)	≥100 (cm)	T0605
Softening Point	49 (°C)	≥47 (°C)	T0606
Dynamic Viscosity (60°C)	≥200 (pa•s)	≥200 (pa•s)	T0620

to be pointed out that the parameters setting of roller cannot be considered because the frequency and amplitude of vibration rolling is determined according to the construction specification. Therefore, the roller setting is kept constant during compaction process to ensure the compaction quality. In addition, to ensure the accuracy of the test, the roller moved at a constant speed when passed the observation point to eliminate the fluctuation of signal for start and deceleration. The schematics of the field test, sensor installation, and rolling site are shown in Figs. 8 and 9.

In the process of asphalt pavement paving, the asphalt mixture is compacted by vibration roller (vibration rolling) for 8 times, and as a matter of fact, after the vibration compaction, the rubber rollers (static rolling) are employed to carry out subsequent compaction, which is not included in this paper and we just focused on the vibration rolling.

(2) Data processing

Owing to the high sensitivity of the SmartRock sensor, multiple vibration signals are collected, such as the signals originating from the pavers and other grouped rollers in the neighboring lanes. For vibratory rollers, the collision and friction of the shafts and bearings generate vibration signals with different frequencies. Significantly, the attenuation of a high-frequency vibration is mixed with a low-frequency vibration, and it is impossible to be differentiated from the above low-

Table 3
Working parameters of vibratory roller.

Operating Weight	Static Weight at Front Drum	Drum dimension: Diameter/width	Frequency	Excited force	Driving speed
13,000 kg	6500 kg	1240 mm × 2140 mm	50 Hz	84 kN	4.5 km/h

frequency signals. Therefore, the signals from the SmartRock and HCF need to be digitally filtered. The filtering conditions are set based on the working frequency of the vibration roller, and the collected data are filtered by the frequency domain method [52]. A band-pass filter code is written with MATLAB, and the measured data are filtered between 48 and 52 Hz, according to the working frequency of the roller, and the low-frequency signals are removed. Finally, the dynamic response data of the asphalt pavement under the vibration roller are obtained. An example band-pass filtering process is displayed in Fig. 10 and the peak value of the dynamic response is illustrated in the histograms of Fig. 11.

In order to analyze the response of pavement during vibration rolling process, the calculation model needs to be calibrated by field test data. The purpose of model calibration, on the one hand, is to determine the value of wave number in the wave number domain; on the other hand, the dynamic modulus of asphalt mixture in the rolling process can be calibrated, that to say, it is necessary to back calculate the modulus of asphalt mixture according to the data results of field test.

Based on the pavement structure and material parameters which is substituted into the calculation model, the acceleration curve over time can be obtained, and the fitting curve of its peak value with modulus is shown in Fig. 12. Meanwhile, combining with the field data, the modulus of asphalt mixture can be evaluated through the equation. Furthermore, the acceleration in theoretical and field test is shown as Fig. 13, which shows good agreement between them and the dynamic modulus is back calculated as 94 MPa and 993 MPa for the first and eighth rolling.

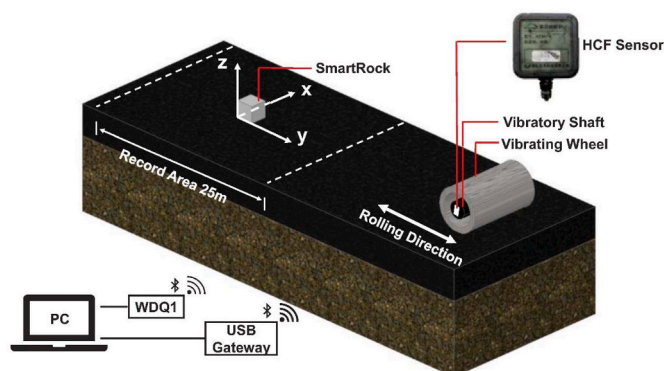


Fig. 8. Diagrams of the field test arrangement and the sensor layout.

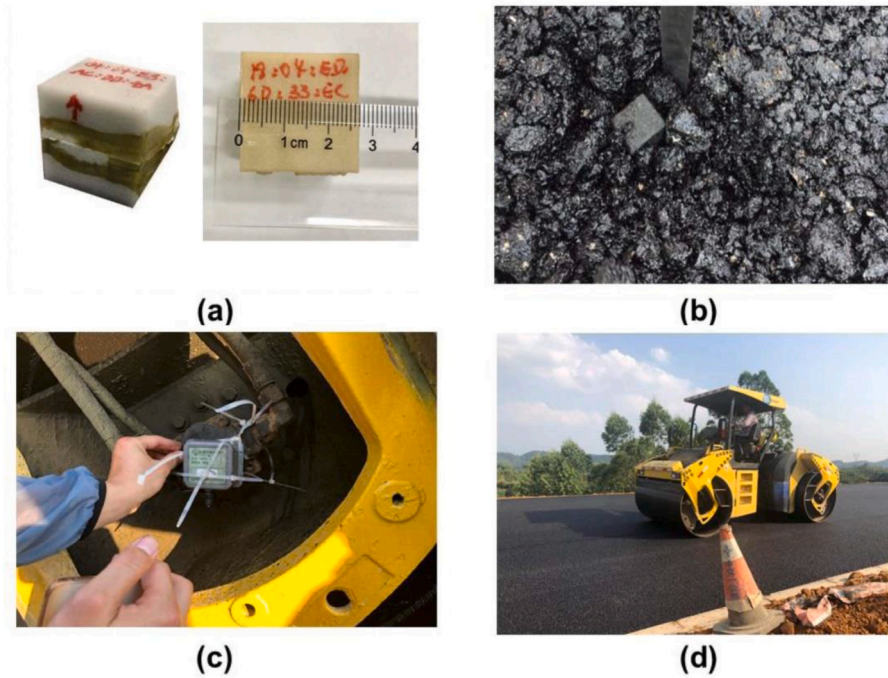


Fig. 9. Field test program: (a) SmarRock size; (b) Embedding of the SmartRock sensor in the asphalt mixture; (c) Installation of an acceleration sensor on the vibrating drum; (d) Pavement rolling

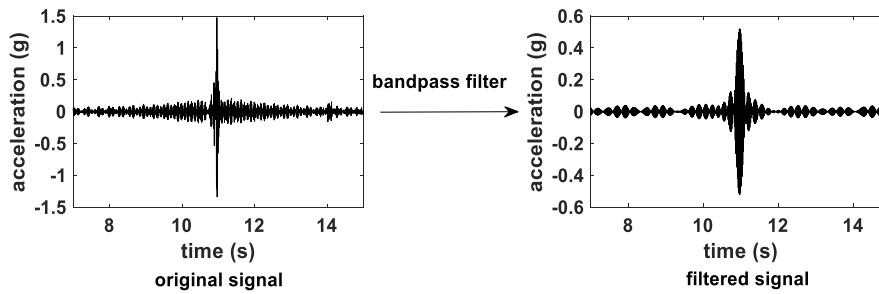


Fig. 10. Band-pass filtering of the measured signal.

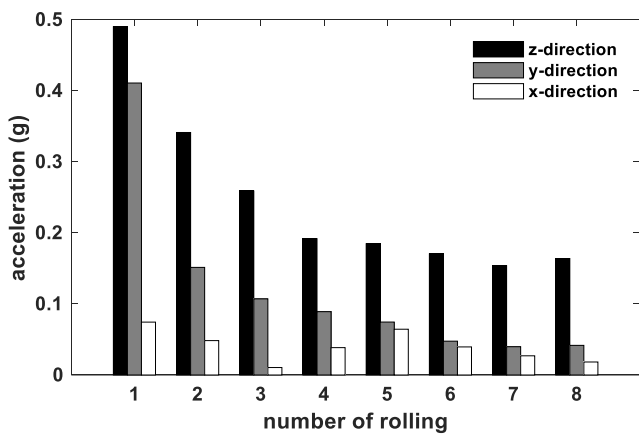


Fig. 11. Peak value of the measured acceleration in various directions in the pavement during the vibration rolling.

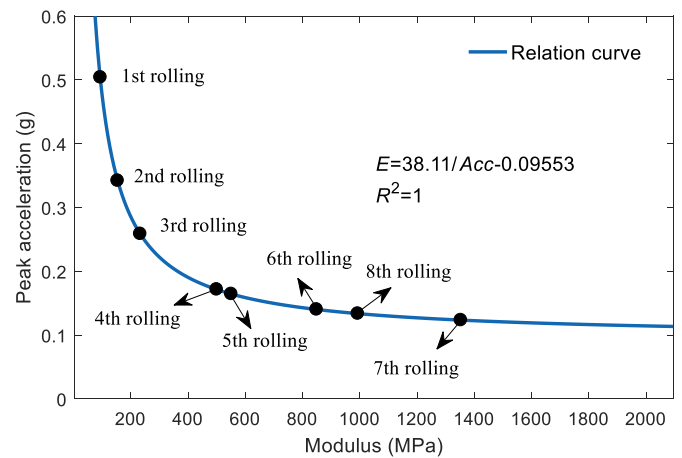


Fig. 12. Fitting curve of peak acceleration and modulus.

(3) Calibration

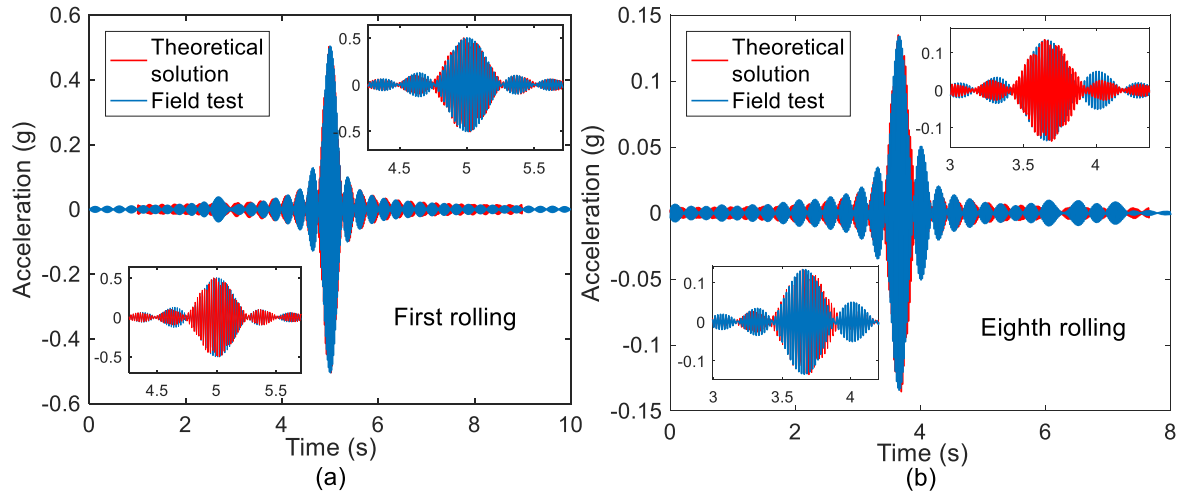


Fig. 13. Acceleration-time curve by calculation and test, (a) is for the first rolling and (b) is for the eighth rolling.

4. Discussion

It should be pointed out that the assumption about the load is that the load does not move but only vibrates with a certain vibration frequency. In actual, the load acting on the asphalt pavement not only vibrates but also moves with a certain speed (e.g., 4.5 km/h to 5.4 km/h) in the engineering practice. As mentioned in Section 2.1, the pavement response with time can be illustrated according to different positions. In other words, when the load vibrates at the initial position x_0 , the dynamic response at position x_1 is equal to that at vibration position x_0 where the load moves to position x_1 .

4.1. Modulus of surface material

As we all know, the modulus of asphalt mixture after paved changes evidently in the process of vibration rolling. On the one hand, the mechanical index such as elastic modulus and strength will increase during the rolling; on the other hand, the changing indexes will have back effect on the dynamic response. In general, the temperature of the paved asphalt mixture is about 135°C–150°C, and it is almost impossible to measure the modulus of the asphalt mixture in the laboratory and field. To date, Chen et al. [53] showed that Burger's model can still be used to simulate the viscoelastic properties of asphalt mixture up to about 150°C. The relationship between dynamic modulus E and model parameters of asphalt mixture can be expressed as follows [54],

$$\frac{1}{E} = \sqrt{\frac{1}{K_{ae}^2} + \frac{1}{\eta_{ae}^2 \omega^2}} + \frac{1 + 2(K_{av}/K_{ae} + \eta_{av}/\eta_{ae})}{K_{av}^2 + \eta_{av}^2 \omega^2} \quad (34)$$

$$K_{ae} = \lim_{\omega \rightarrow \infty} E \quad (35)$$

$$\eta_{av} = \lim_{\omega \rightarrow 0} \frac{E}{\omega} \quad (36)$$

where ω is the angular frequency; K_{ae} and η_{ae} are the modulus and viscosity of the spring and dashpot elements in serial of Burger's model; K_{av} and η_{av} are the modulus and viscosity of the spring and dashpot elements in parallel of Burger's model.

Liu et al. [54] developed an iterative program. Through nonlinear regression analysis, the relationships between model parameters and temperature, porosity and loading frequency were established, therefore, equations (34)–(36) can be used to determine the modulus of asphalt mixture at any temperature and density [55]. From the paving to compaction of asphalt mixture, the predicted range of modulus is 100

MPa–3000 MPa according to the above-mentioned model [54]. Therefore, the modulus of asphalt mixture can be approximately determined to analyze its effect on the dynamic response. The material and structure information can refer to Table 4. Herein, it is pointed out that the vertical acceleration and vertical displacement of pavement is the main concern in this paper.

(1) vertical acceleration

During the vibration rolling, the acceleration of pavement surface can be applied to characterize the dynamic response of asphalt mixture under vibrating load. Fig. 14 shows the vertical acceleration time history curve with different modulus of the upper layer of pavement. It can be seen from the figure that the acceleration changes evidently when the vibrating wheel approaches the observation point. Although there is also a change of acceleration far from the observation point, the change amplitude is much too small. The amplitude of acceleration begins to increase gradually when the load moves from the origin about 1.0 s (about 1.25 m) to the observation point, and the acceleration reaches the peak value when the load center moves to the observation point. Therefore, the acceleration response range of the observation point is about 2s (2.5 m).

In order to analyze the variation trend of the peak acceleration of the road surface with the modulus of the upper layer, several maximum values of acceleration are calculated and shown in Fig. 15. Apparently, with the continuous increase of modulus from 100 MPa to 3000 MPa, the peak acceleration of pavement surface decreases gradually from 0.9312g to 0.1849g, which decreases by about 80.14%. By the fitting curve between the acceleration and modulus, the decreasing speed of

Table 4
Structure and material information for tested pavement.

Materials	Thickness (cm)	Dynamic modulus (MPa)	Poisson's ratio	Density (kg/m ³)
Asphalt mixture (lower course)	8	calibration	0.30	2600
Cement stabilized macadam (5% cement content)	26	3500	0.25	2600
Cement stabilized macadam (4% cement content)	20	3450	0.25	2600
Graded aggregate	16	300	0.30	2550
Subgrade soil	100	45	0.35	1850

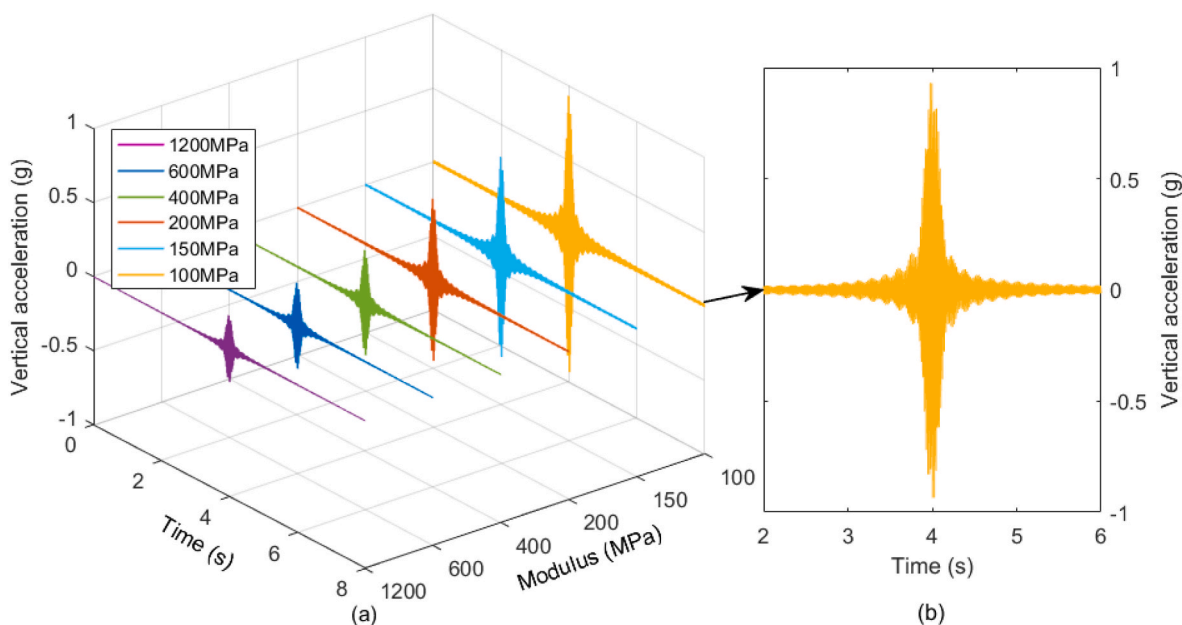


Fig. 14. Time-acceleration curves for different modulus of upper-layer materials.

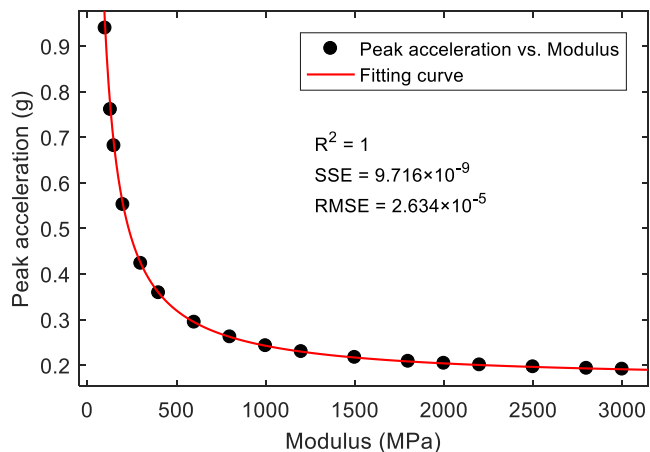


Fig. 15. Relation curve between peak acceleration and modulus of pavement.

the peak acceleration is getting smaller. According to the field test of pavement compaction [50], the peak acceleration between former three rolling time (initial compaction in terms of engineering) changes remarkably, and the acceleration in 3rd rolling is about 0.24g, which approximately corresponds to the peak acceleration when modulus is 1000 MPa in this paper. Similarly, the peak acceleration of the last rolling in second stage is about 0.17g, which corresponds to material modulus of 2500 MPa. Thus, the fitting curve can be divided into three stages: rapid decline, slow decline and stable stages.

The first is rapid decline stage. The peak acceleration decreased from 0.9312g to 0.2364g which decreases by 74.61%, and the corresponding material modulus increased from 100 MPa to 1000 MPa which increases by 900 MPa. From the engineering point of view, the particles in the asphalt mixture move violently to form a more stable structure which is changed from the loose state to a dense state during the compaction process.

The second is the general decline stage. The peak acceleration decreases from 0.2364g to 0.1901g, and the corresponding modulus

increases from 1000 MPa to 2500 MPa, which increases by 1500 MPa, while the peak acceleration decreased by about 19.59%. Similarly, from the construction point of view, after several rolling times, the asphalt mixture gradually has strength of resistance to external force, and the particle movement has also become gentle and the mixture gets denser.

The third is stable stage. When the material modulus increases from 2500 MPa to 3000 MPa, the peak acceleration only decreases by about 2.74%, indicating that the peak acceleration of the pavement tends to be stable, which can reflect that the particles of the mixture are difficult to move after the asphalt mixture reaches a higher degree of compaction.

According to the curve fitted by the scatter plot in Fig. 15, it is obvious that there is a non-linear relationship between the peak acceleration and the modulus of the upper layer, which can be expressed by

$$Acc = \frac{77.22}{E} + 0.1592 \tag{37}$$

in which correlation coefficient equals to 1, and *Acc* is the peak acceleration of the road surface [g], *E* is the modulus of the upper layer material [MPa].

(2) vertical displacement

In addition to the acceleration, the dynamic response of the vertical displacement of pavement surface is also obvious. Fig. 16 shows the vertical displacement curve of the observation point under the condition of different modulus of the upper layer material, and Fig. 17 is the scatter diagram of the corresponding peak value of vertical displacement and the fitting curve.

Likewise, the displacement vibrates regularly and fluctuates around 0. Furthermore, it can be found in Fig. 16 (a) that the response range of vertical displacement decreases gradually with the increase of modulus. For instance, when the modulus is 100 MPa, the response range of vertical displacement is about 3.125 m, while it is about 0.833 m for 1200 MPa. The range is reduced by 73.34%. From the engineering view of point, it is rational. On the one hand, when the modulus goes up, the compaction degree and strength also increase, and the particles of asphalt mixture is hard to move; on the other hand, the negative displacement indicates that the uplift of pavement surface occurs near

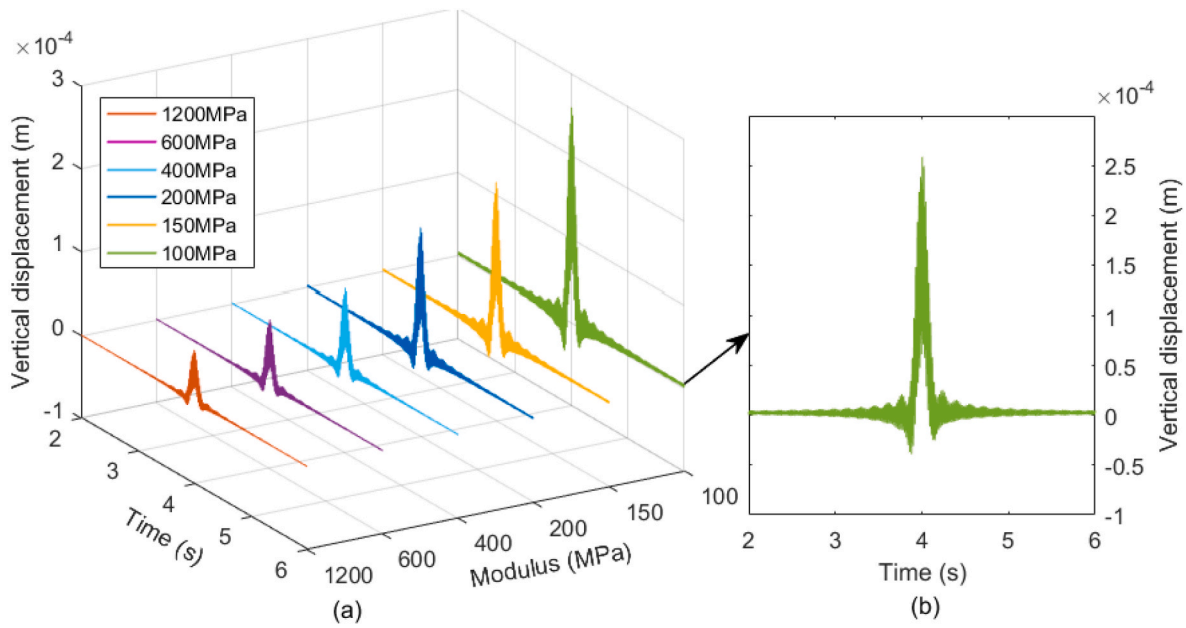


Fig. 16. The displacement-time curves for different modulus of upper layer.

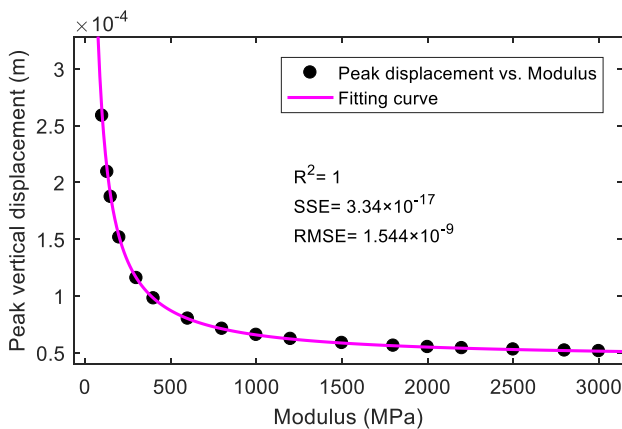


Fig. 17. The relationship between the peak vertical displacement and modulus.

the area of the observation point when it is subjected to the moving vibration load.

In addition, it can be seen from Fig. 17 that the peak vertical displacement of the pavement also shows a sharp downward trend at first. For instance, when the modulus increases from 100 MPa to 1000 MPa, the peak vertical displacement decreases from 2.59×10^{-4} m to 6.57×10^{-5} m with a decrease of about 74.63%, and then the decline rate gradually slows down with the increase of the modulus. Finally, it tends to be stable.

With the comparison of Figs. 15 and 17, the variation trend of peak vertical displacement with modulus is similar to that of peak acceleration. Therefore, the relationship between peak vertical displacement and material modulus can also be expressed in the form of equation (37) as follows.

$$u_z = \frac{0.02144}{E} + 4.422 \times 10^{-5} \quad (38)$$

where, correlation coefficient equals to 1, and u_z is the peak value of vertical displacement [m], E is the modulus of the upper layer [MPa].

4.2. Base material modulus

Generally speaking, the asphalt pavement is essentially a multi-layer system, and it is basically constructed layer by layer in the practice. For the typical pavement structure, the surface course of asphalt mixture is located above the base course (e.g., flexible base, semi-rigid base, rigid base). As we known, different base materials have different strength, stiffness and modulus. Therefore, in addition to the consideration of modulus influence of surface course on the acceleration and displacement of the pavement surface, the base course cannot be ignored, and the influence of the modulus of base material on the acceleration and vertical displacement of pavement surface (the modulus of the surface course is kept 1400 MPa in the calculation). As shown in Fig. 18, the relationships of the peak acceleration and displacement with the base modulus are significantly nonlinear as well, and it can be also expressed in the form of equations (37) and (38)

$$\begin{cases} Acc = \frac{103.8}{E_{sub}} + 0.145 \\ u_z = \frac{0.02886}{E_{sub}} + 4.029 \times 10^{-5} \end{cases} \quad (39)$$

where, the correlation coefficients of two equations both equal to 1, and Acc is the peak value of acceleration of pavement surface [g], u_z is the peak vertical displacement [m], and E_{sub} is the modulus of base material [MPa].

It can be seen from Fig. 18 that when the modulus of base course increases 19 times from 200 MPa, the peak value of acceleration and vertical displacement decrease steeply at first and then slowly, in which the peak acceleration decreases from 0.6647g (6.55 ms^{-2}) to 0.171g (1.68 ms^{-2}), and the peak vertical displacement decreases from 1.85×10^{-4} m to 4.75×10^{-5} m by about 74%.

According to Figs. 14–18, it can be seen that the change of the modulus of any layers in the multi-layer system will lead to the corresponding variation of the dynamic response of the pavement such as the acceleration and displacement of the pavement. It is significant that the influence of modulus on the acceleration and displacement of pavement surface can be of the following form

$$Acc \text{ or } u_z = \frac{a}{E_i} + b \quad (40)$$

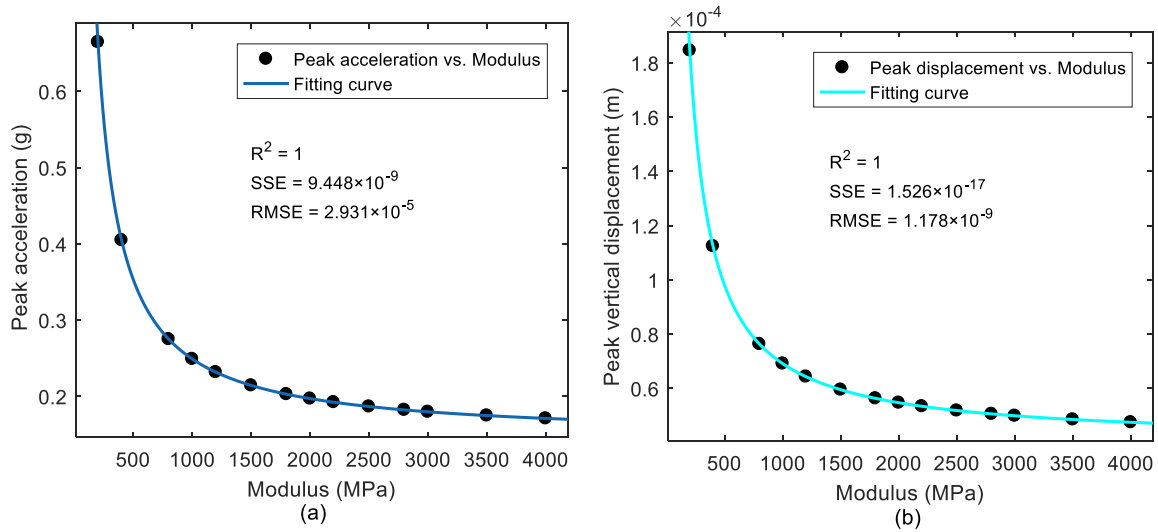


Fig. 18. Effect of base material modulus on dynamic response.

in which the subscript *i* represents the layer type, i.e., surface course, base course, etc.

It is worth pointing out that if try to measure the acceleration or displacement on the pavement surface and establish a relation with the compaction degree between them, it is bound to be affected by the type of the base course, namely the modulus of the base layer. In this paper, the regulation of the influence is proved to be a nonlinear influence as shown in equation (40).

4.3. Vibrating frequency

Different from material modulus, load is the most significant external factor. The vibrating frequency almost determines the excitation force of

the vibratory roller. Therefore, to analyze the influence of vibrating frequency in the process of rolling, the frequency varies between 25 Hz and 50 Hz without changing the material parameters, and the calculation results of acceleration and displacement are shown in Fig. 19.

For the peak acceleration shown in Fig. 19, it grows up obviously with the increase of the vibrating frequency. When the frequency goes up from 25 Hz to 50 Hz, the peak acceleration increases from 0.0218g to 0.2378g with about 9.9 times higher. According to the fitting curve of the scatter diagram (Fig. 20), it can be seen that there is a quadratic relationship between the peak acceleration and the frequency, which can be expressed by equation (41).

$$Acc = 2.201 \times 10^{-4}f^2 - 7.852 \times 10^{-3}f + 0.08097 \tag{41}$$

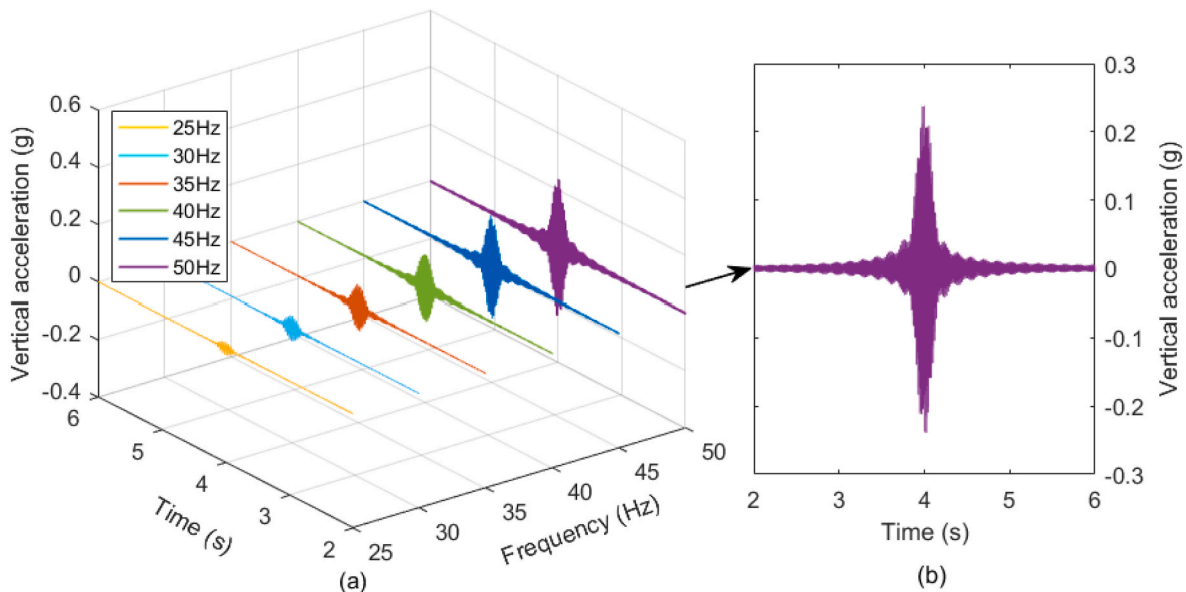


Fig. 19. Acceleration-time curve under different frequency loads.

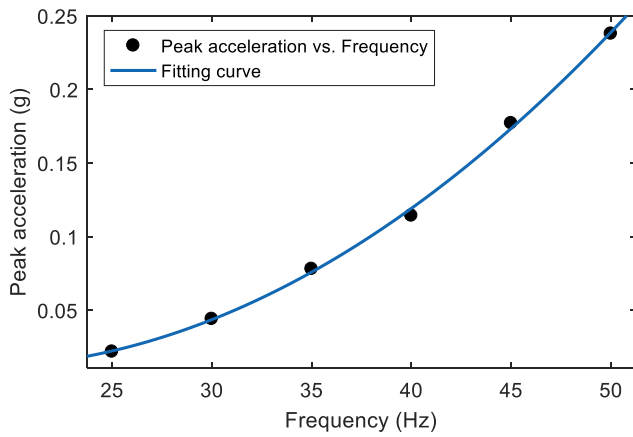


Fig. 20. Relationship between peak acceleration and load frequency.

where, the correlation coefficient equals 0.9987, Acc and f are the peak acceleration [g] and vibrating frequency [Hz] of load, respectively.

Meanwhile, the vertical displacement response under different frequency loads is analyzed and shown in Fig. 21. Fig. 21 (a) shows the vertical displacement response curve under different load vibration frequencies at the observation point, and Fig. 21 (b) shows the relationship between the peak value of vertical displacement and the load frequency.

It can be seen from Fig. 21(a) that the vibration frequency of vertical displacement goes up with the increase of load frequency and the response range and displacement amplitude at the observation point also increase. The main reason is that the exciting force of vibratory roller magnifies with the increase of vibration frequency. For instance, when the load vibration frequency increases from 25 Hz to 50 Hz, the variation law of the peak value of vertical displacement and its fitting curve are shown in Fig. 21 (b). Evidently, there is also an obvious quadratic correlation between them, and the relationship can be established similar to the peak acceleration as follows.

$$u_z = 2.067 \times 10^{-8} f^2 - 6.378 \times 10^{-7} f + 4.438 \times 10^{-5} \quad (42)$$

where, the correlation coefficient equals 0.9936, u_z is peak vertical displacement [m], and f is the load vibration frequency [Hz].

From equations (41) and (42), it can be inferred that the peak

acceleration and vertical displacement of the pavement surface are quadratic related to the load frequency, that is,

$$Acc \text{ or } u_z = a \times f^2 + b \times f + c \quad (43)$$

In summary, from the analysis results of the influencing factors (i.e., modulus and frequency), the proposed equation (40) and equation (43) can reflect the regulation of influencing factors on the acceleration and displacement of the pavement surface under vibrating load. It should be pointed out that the acceleration and displacement of the pavement surface are the physical quantities obtained by the possibility test during the vibration rolling of the pavement, which provides a way to characterize the compactness of the compacted material of the pavement. For example, the method of inverse calculation of the modulus of asphalt mixture can be explored. Therefore, equation (40) and equation (43) provide theoretical and technical support for accurately determining and modifying some indexes that characterize the compaction degree of asphalt pavement.

5. Summary and conclusion

- (1) In this paper, investigations have been carried out to study the dynamic response of pavement structure under vibrating load during the process of vibrating rolling. Based on the viscoelastic theory of layered system, a set of differential governing equation of dynamic response is established under the vibration rolling load, which is simplified by Fourier transform method in the form of matrix.
- (2) Further, the stiffness matrixes of single-layer structure and multi-layer system are derived, and the dynamic stiffness method is applied to solve the governing equation of multi-layer pavement structure under vibrating load. The proposed solution is validated by the FEM simulation and analytical method, which is proved to be more efficient. Furthermore, the theoretical model is calibrated by the field test to determine the wave number and dynamic modulus during the vibration rolling process.
- (3) The regulation of dynamic response of pavement is explored with respect to the acceleration and displacement of pavement surface. Both of them show the obviously periodic fluctuation and damping at the observation point during vibrating rolling process. The peak value of acceleration and displacement is apparent and rapidly decline before and after the observation point.

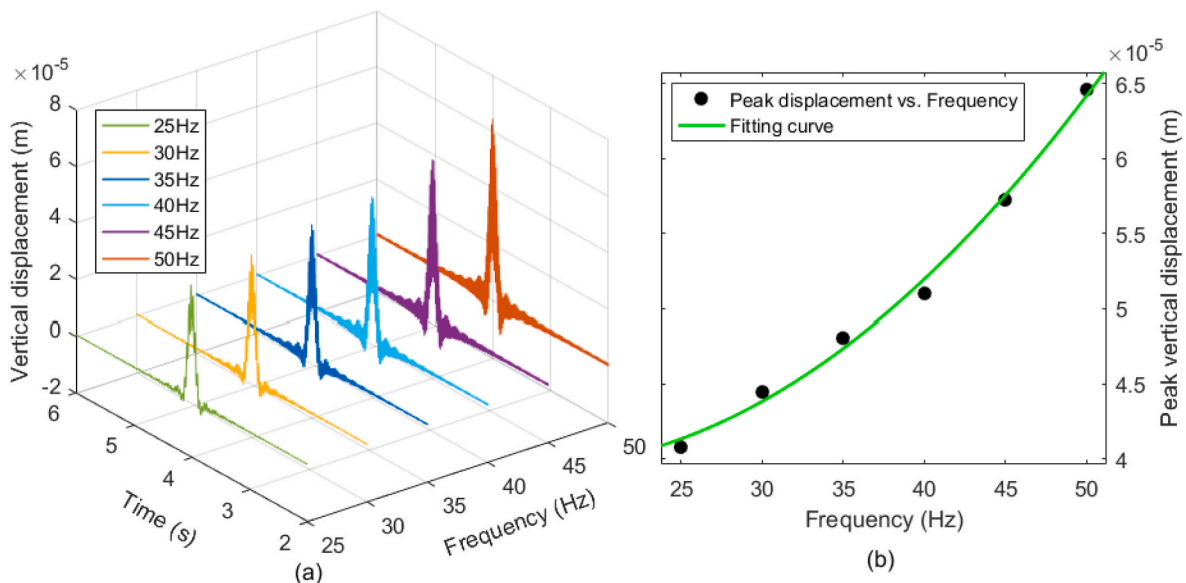


Fig. 21. Influence of load frequency on the vertical displacement.

- (4) Through the analysis of influencing factors in terms of the modulus of pavement materials, not only the paved surface course but also the base course, the relationships of the acceleration and displacement with modulus are established and of the form power function $f(x) = a/x + b$. Meanwhile, three stages (i.e., rapid decline, general decline and stable stages) of acceleration of pavement surface are proposed to illustrate the effect of modulus of surface course with respect to the engineering practice.
- (5) Finally, the influence of vibrating frequency of load is investigated and the results show that the peak values of vertical displacement and acceleration are quadratic with the load frequency which can be expressed by the formed equation $f(x) = ax^2 + bx + c$.

It should be pointed out that the compaction process of asphalt pavement is a very complex process. As we all know, in practical engineering, modulus and density are the coupling physical parameters for a certain temperature. Generally speaking, the density increases gradually and the modulus increases gradually during the rolling process. However, the temperature is continuous falling down during the rolling process. There is not a definite relation between the modulus and density of the pavement mixture. In reality and practice, the density change is small and the range of change is about 5% of the maximum theoretical density, while the change of modulus is more significant and there will be more than 10 times of change. Therefore, the density and modulus are decoupled in this paper due to the little effect of density on the dynamic response of pavement. We think that the elastic theory to study the density or porosity on the modulus and the compaction degree of asphalt mixture is not meaningless, and the study by the DEM need to be developed in the future. Nevertheless, this paper provides an insight into understanding the dynamic response of pavement under vibration rolling condition to some extent, and potentially provides theoretical and technical support for accurately determining and modifying some indexes that characterize the compaction degree of asphalt pavement.

Funding

This research was supported by the National Natural Science Foundation of China (Grant No. 51908558), the Hunan Transportation Science and Technology Foundation of China (Grant No. 201622), the Natural Science Foundation of Hunan Province of China (Grant No. 2020JJ4702), and the Guizhou Transportation Science and Technology Foundation of China (Grant No. 2019-122-006).

Disclosure statement

- The authors declare that they have no conflict of interest.
- All the data for analysis has been included in the article.

CrediT author statement

Shi-Ping Wang: Methodology, Writing- Original draft preparation, Investigation; **Han-Cheng Dan:** Conceptualization, Methodology, Funding acquisition, Writing- Reviewing and Editing; **Liang Li:** Supervision, Writing- Reviewing and Editing. **Xiang Liu:** Supervision, Writing- Reviewing and Editing; **Zhi Zhang:** Investigation, Resources.

Declaration of competing interest

The authors declare that they have no conflict of interest.

References

- [1] Zaumanis M, Poulikakos L, Partl M. Performance-based design of asphalt mixtures and review of key parameters. *Mater Des* 2018;141:185–201.
- [2] Dan HC, He LH, Zhao LH. Experimental investigation on the resilient response of unbound graded aggregate materials by using large-scale dynamic triaxial tests. *Road Mater Pavement Des* 2020;21(2):434–51.
- [3] Dan HC, Tan JW, Du YF, Cai JM. Simulation and optimization of road deicing salt usage based on Water-Ice-Salt Model. *Cold Reg Sci Technol* 2020;169:102917.
- [4] Hosseini A, Faheem A, Titi H, Schwandt S. Evaluation of the long-term performance of flexible pavements with respect to production and construction quality control indicators. *Construct Build Mater* 2020;230:116998.
- [5] Wang H, Zhang Q, Tan J. Investigation of layer contributions to asphalt pavement rutting. *J Mater Civ Eng* 2009;21(4):181–5.
- [6] Dan HC, Tan JW, Chen JQ. Temperature distribution of asphalt bridge deck pavement with groundwater circulation temperature control system under high- and low-temperature conditions. *Road Mater Pavement Des* 2019;20(3):509–27.
- [7] Dan HC, Zhang Z, Liu X, Chen JQ. Transient unsaturated flow in the drainage layer of a highway: solution and drainage performance. *Road Mater. Pavemnet Des.* 2019;20(3):528–53.
- [8] Wu HN, Li P, Nian TF, Zhang GH, He T, Wei XY. Evaluation of asphalt and asphalt mixtures' water stability method under multiple freeze-thaw cycles. *Construct Build Mater* 2019;228:117089.
- [9] Jing C, Zhang JX, Song B. An innovative evaluation method for performance of in-service asphalt pavement with semi-rigid base. *Construct Build Mater* 2020;235:117376.
- [10] Coleri E, Harvey JT, Yang K, Boone JM. A micromechanical approach to investigate asphalt concrete rutting mechanisms. *Construct Build Mater* 2012;30:36–49.
- [11] Xu QX, Chang G. Adaptive quality control and acceptance of pavement material density for intelligent road construction. *Autom Construct* 2016;62:78–88.
- [12] Jia T, He TJ, Qian ZD, Lv J, Cao KX. An improved low-cost continuous compaction detection method for the construction of asphalt pavement. *Adv Civ Eng* 2019;2019:1–11.
- [13] Liu DH, Chen JJ, Li S. Collaborative operation and real-time control of roller fleet for asphalt pavement compaction. *Autom Construct* 2019;98:16–29.
- [14] Hu W, Jia XY, Zhu XY, Gong HR, Xue GP, Huang BS. Investigating key factors of intelligent compaction for asphalt paving: a comparative case study. *Construct Build Mater* 2019;229:116876.
- [15] Hu W, Huang BS, Shu X, Woods M. Utilising intelligent compaction meter values to evaluate construction quality of asphalt pavement layers. *Road Mater Pavement Des* 2017;18(4):980–91.
- [16] Liu PF, Wang DW, Oeser M. Application of semi-analytical finite element method to analyze asphalt pavement response under heavy traffic loads. *J Traffic Transport Eng* 2017;4(2):206–14.
- [17] Dan HC, He LH, Zhao LH, Chen JQ. Coupled hydro-mechanical response of saturated asphalt pavement under moving traffic load. *Int J Pavement Eng* 2015;16(2):125–43.
- [18] Dan HC, Zou ZM, Chen JQ, Peng AP. DEM-aided method for predicting the hydraulic properties with particle-size distribution of porous media. *Eng Comput* 2019;36(5):1716–43.
- [19] Lyu Z, Qian JG, Shi ZH, Gao Q. Dynamic responses of layered poroelastic ground under moving traffic loads considering effects of pavement roughness. *Soil Dynam Earthq Eng* 2020;130:105996.
- [20] Peng AP, Dan HC, Yang D. Experiment and numerical simulation of the dynamic response of bridges under vibratory compaction of bridge deck asphalt pavement. *Math Probl Eng* 2019:1–16 (2019).
- [21] Li MY, Wang H, Xu GJ, Xie PY. Finite element modeling and parametric analysis of viscoelastic and nonlinear pavement responses under dynamic FWD loading. *Construct Build Mater* 2017;141(141):23–35.
- [22] Assogba OC, Sun ZQ, Tan YQ, Nonde L, Bin Z. Finite-element simulation of instrumented asphalt pavement response under moving vehicular load. *Int J Geomech* 2020;20(3):04020006.
- [23] Gao LS, Dan HC, Li L. Response analysis of asphalt pavement under dynamic loadings: loading equivalence. *Math Probl Eng* 2019;2019:1–15.
- [24] Li HT, Wang GQ, Qin LS, Wang QK, Wang XQ. A spectral analysis of the dynamic frequency characteristics of asphalt pavement under live vehicle loading. *Road Mater Pavement Des* 2020;21(2):486–99.
- [25] Shan JS, Shao HM, Li QZ, Sun PL. Comparison of real response and theoretical modeling of pavement with thick asphalt layers under heavy traffic load. *Adv Civ Eng* 2019;2019:1–11 (2019).
- [26] Chen XB, Zhang JS, Wang X. Full-scale field testing on a highway composite pavement dynamic responses. *Transp. Geotech.* 2015;4:13–27.
- [27] Steenbergen M, Metrikine A. The effect of the interface conditions on the dynamic response of a beam on a half-space to a moving load. *Eur J Mech Solid* 2007;26(1):33–54.
- [28] Kononov A, Wolfert R. Load motion along a beam on a viscoelastic half-space. *Eur J Mech Solid* 2000;19(2):361–71.
- [29] Dong ZJ, Ma XY. Analytical solutions of asphalt pavement responses under moving loads with arbitrary non-uniform tire contact pressure and irregular tire imprint. *Road Mater Pavement Des* 2018;19(8):1887–903.
- [30] Lin S, Shen YC. Stress fields of a half-plane caused by moving loads-resolved using doublet mechanics. *Soil Dynam Earthq Eng* 2005;25(12):893–904.
- [31] Grundmann H, Lieb M, Trommer E. The response of a layered half-space to traffic loads moving along its surface. *Arch Appl Mech* 1999;69(1):55–67.
- [32] Xu B, Lu JF, Wang JH. Dynamic response of a layered water-saturated half space to a moving load. *Comput Geotech* 2008;35(1):1–10.
- [33] Xu B, Lu JF, Wang JH. Dynamic response of an infinite beam overlying a layered poroelastic half-space to moving loads. *J Sound Vib* 2007;306(1):91–110.
- [34] Lu JF, Jeng D. A half-space saturated poro-elastic medium subjected to a moving point load. *Int J Solid Struct* 2007;44(2):573–86.

- [35] Jin B, Yue ZQ, Tham LG. Stresses and excess pore pressure induced in saturated poroelastic halfspace by moving line load. *Soil Dynam Earthq Eng* 2004;24(1):25–33.
- [36] Lefeuvemesgouez G, Mesgouez A. Ground vibration due to a high-speed moving harmonic rectangular load on a poroviscoelastic half-space. *Int J Solid Struct* 2008;45(11):3353–74.
- [37] Beskou N, Hatzigeorgiou G, Theodorakopoulos D. Dynamic inelastic analysis of 3-D flexible pavements under moving vehicles: a unified FEM treatment. *Soil Dynam Earthq Eng* 2016;82:420–31.
- [38] Imran S, Commuri S, Barman M, Zaman M, Beainy F. Modeling the dynamics of asphalt-roller interaction during compaction. *J Construct Eng Manag* 2017;143(7):04017015.
- [39] Susante PV, Mooney M. Capturing nonlinear vibratory roller compactor behavior through lumped parameter modeling. *J Eng Mech* 2008;134(8):684–93.
- [40] Ministry of Transport of the People's Republic of China. Technical specification for construction of highway asphalt pavement, JTG F-40. Beijing, Chian: China Communication Press; 2004.
- [41] Zhong Y, Geng LT. Explicit solution of multiplayer elastic plane by exact stiffness matrix method. *Rock Soil Mech* 2008;29(10):2829–32.
- [42] Yan KZ, Shi TW, You LY, Man JH. Spectral element method for dynamic response of multilayered half medium subjected to harmonic moving load. *Int J Geomech* 2018;18(12):04018161.
- [43] Herrera C, Costa PA, Caicedo B. Numerical modelling and inverse analysis of continuous compaction control. *Transp. Geotech.* 2018;17:165–77.
- [44] Bratu P, Dobrescu C. Dynamic response of zener-modelled linearly viscoelastic systems under harmonic excitation. *Symmetry* 2019;11(8):1050.
- [45] Wang N, Zhang Z, Zhang X. Stiffness analysis of corrugated flexure beam using stiffness matrix method. *Proc Inst Mech Eng Part C-J Eng Mech Eng Sci* 2019;233(5):1818–27.
- [46] Khavassefat P, Jelagin D, Birgisson B. Dynamic response of flexible pavements at vehicle–road interaction. *Road Mater Pavement Des* 2015;16(2):256–76.
- [47] Liu X, Zhao X, Xie C. Exact free vibration analysis for membrane assemblies with general classical boundary conditions. *J Sound Vib* 2020;485:115484.
- [48] Liu X, Sun C, Banerjee JR, Dan HC, Chang L. An exact dynamic stiffness method for multibody systems consisting of beams and rigid-bodies. *Mech Syst Signal Process* 2021;150:107264.
- [49] Zhong Y, Chen J, Wang L, Li Y. Explicit solution for dynamic response of asisymmetrical problem in multilayered viscoelastic half space by exact stiffness matrix method. *Chin J Comput Mech* 2003;20(6):749–55.
- [50] Dan HC, Yang D, Liu X, Peng AP, Zhang Z. Experimental investigation on dynamic response of asphalt pavement using SmartRock sensor under vibrating compaction loading. *Construct Build Mater* 2020;247:118592.
- [51] Ministry of Transport of the People's Republic of China. Standard test methods of bituminous mixtures for highway engineering, JTG E20. Beijing, China: China Communications Press; 2019.
- [52] Chen L, Zheng HP. A comparative study of the time and frequency domains in dynamic analysis of vibratory roller. *Journal of Shijiazhuang University of Applied Technology* 2014;26(6):36–9.
- [53] Chen JS, Huang BS, Shu X. Air-void distribution analysis of asphalt mixture using discrete element method. *J Mater Civ Eng* 2013;25(10):1375–85.
- [54] Liu Y, Dai QL, You ZP. Viscoelastic model for discrete element simulation of asphalt mixtures. *J Eng Mech* 2009;135(4):324–33.
- [55] Beainy F, Commuri S, Zaman M. Dynamical response of vibratory rollers during the compaction of asphalt pavements. *J Eng Mech* 2014;140(7):04014039.